Molecular quantitative trait loci in reproductive tissues impact male fertility in a large mammal

Xena Marie Mapel[1,*], Naveen Kumar Kadri [1,*], Alexander S. Leonard [1], Qiongyu He [1], Audald Lloret-Villas [1], Meenu Bhati [1,$], Maya Hiltpold [1,&], Hubert Pausch [1,#]

[1] Animal Genomics, ETH Zurich, Universitatstrasse 2, 8092 Zurich, Switzerland
[$] current address: Roslin Institute, The University of Edinburgh, Easter Bush Campus, Midlothian EH25 9RG, United Kingdom
[&] current address: GenPhySE, Université de Toulouse, INRAE, ENVT, 31326, Castanet Tolosan, France

[*] equal contribution
[#] Corresponding author

Abstract

Cattle are well suited to investigate inherited variation in male fertility because insemination success is recorded in thousands of artificial insemination bulls. However, functional data from relevant tissues are lacking, which prevents fine-mapping fertility-associated genomic regions to reveal functional links between genotype and phenotype. Here, we profile testis, epididymis, and vas deferens transcriptomes in 118 mature bulls and conduct association tests between 417k molecular phenotypes and more than 21M genome-wide variants to identify 41k regulatory loci. We show that expression- and splicing-mediating variants are more than three times as frequent in testis than epididymis and vas deferens, highlighting the transcriptional complexity of testis. We identify genes (*WDR19*, *SPATA16*, *KCTD19*, *ZDHHC1*) and molecular phenotypes that are associated with male fertility through transcriptome-wide association studies and colocalization analyses, revealing molecular-genetic underpinnings of quantitative variation in male fertility.

Introduction

Male fertility varies considerably between individuals, but it remains difficult to identify underlying genetic mechanisms (Tüttelmann et al., 2018; Xavier et al., 2021). Exploring the genetic basis of reproductive success requires separating genetic from environmental effects and differentiating between male and female factors that contribute to fertilization; this is only possible when repeated phenotypic measurements are available for large cohorts. While such cohorts are unavailable for nearly all species, including humans, the beef and dairy industries' reliance on artificial insemination has generated comprehensive catalogs of semen quality and male fertility records for thousands of genotyped artificial insemination bulls (Thibier & Wagner, 2002). Indeed, studies investigating bull fertility have high translational value as they can elucidate evolutionarily conserved functional mechanisms that contribute to undisturbed mammalian fertilization (Lamas-Toranzo et al., 2020; Pausch et al., 2014; Tang et al., 2022), making cattle an unconventional—but ideally suited—species to study the genetic architecture of male reproductive ability.

Bovine male reproductive traits have low-to-moderate heritability, suggesting they are amenable to association testing with dense molecular markers (Butler et al., 2020; Gebreyesus et al., 2021; Nagai et al., 2022; Pausch & Mapel, 2023). Datasets from artificial insemination bulls provide enough statistical power to identify variants that contribute to inherited variation in male fertility through genome-wide association studies (GWAS). Several thousand quantitative trait loci (QTL) for male reproductive traits are listed in the AnimalQTL Database (https://www.animalgenome.org/cgi-bin/QTLdb/index); many of these loci are in non-coding regions of the genome and segregate within populations at relatively high frequencies (Han & Peñagaricano, 2016; Nicolini et al., 2018; Pacheco et al., 2022; Rezende et al., 2018). Though numerous male fertility QTL have been identified in cattle, a lack of functional data has caused the molecular underpinnings for most of these loci to remain elusive (Druet et al., 2009; Hiltpold et al., 2021; Rezende et al., 2018).

Variants that regulate gene expression and splicing influence complex traits and diseases (Garrido-Martín et al., 2021; Y. I. Li et al., 2016; Walker et al., 2019; Yamaguchi et al., 2022). Several Genotype-Tissue Expression (GTEx) projects identified thousands of regulatory molecular quantitative trait loci (molQTL; specifically expression and splicing QTL) throughout mammalian genomes for dozens of tissues (GTEx Consortium, 2020; Liu et al., 2022; The FarmGTEx-PigGTEx Consortium et al., 2022). Integration of molQTL and phenotypic records, or summary statistics from

GWAS, through transcriptome-wide association studies (TWAS) can identify regulatory variants that are associated with complex trait variation (Barbeira et al., 2018; Wainberg et al., 2019; Wu et al., 2019). However, since this requires uniform cohorts with detailed trait records and transcriptomics data for functionally relevant tissues, TWAS for male fertility have not been feasible thus far.

Here, we establish a large and homogeneous cohort of bulls that contains both DNA sequencing and transcriptome data from testis, epididymis, and vas deferens. We characterize the transcriptomic profile of these three reproductive tissues and identify thousands of loci that influence gene expression and splicing. In doing so, we discover an excess of regulatory small-effect variants in testis that are often tissue specific. Lastly, we conduct transcriptome-wide association studies and colocalization analyses to pinpoint molecular phenotypes that impact bovine male fertility.

Results

We sampled testis, epididymis (caput), and vas deferens tissue from 118 bulls of Braunvieh (BV) ancestry (i.e., Brown Swiss (BS), Original BV (OB), or a cross between one of these and a different breed; Figure 1A;1B;1C; Figure S1). All bulls were considered post-pubertal, although the age at sampling varied from 10 to 37 months. Whole-genome sequencing (WGS) of DNA extracted from testis tissue yielded between 65,207,590 and 461,834,248 cleaned paired-end reads per sample (mean = 208,761,950 ± 63,260,972). The subsequent alignment of these reads against the *Bos taurus* reference genome achieved an average coverage of 12.34 ± 3.71 -fold. Variant calling identified 29,660,795 polymorphic sites (single nucleotide polymorphisms (SNPs), insertions and deletions (indels) smaller than 50 bp), of which 21,501,032 met our quality criteria for downstream analyses (Table S1).

Total RNA from testis, epididymis, and vas deferens tissue was extracted from the same bulls and sequenced with stranded paired-end libraries. We used a splice-aware alignment tool to map an average of 257,050,199, 283,746,666, and 262,089,072 reads per sample for testis, epididymis, and vas deferens, respectively, to the bovine reference genome and the Ensembl gene annotation (Table S2). An additional set of alignments that included WASP filtering (Van De Geijn et al., 2015) to mitigate reference allele bias contained an average of 240,544,139 mapped reads in testis, 267,645,035 mapped reads in epididymis, and 251,031,216 mapped reads in vas deferens (Table S2).

Our final dataset contained 117, 103, and 84 samples for testis, epididymis, and vas deferens, respectively, 74 of which had data of sufficient quality for all three tissues (Figure 1A; 1B).

Gene expression and splicing variation is pervasive in male reproductive tissues

We estimated gene expression in transcripts per million (TPM) and, after filtering, detected 21,844 expressed genes (≥ 0.1 TPM and ≥ 6 reads in ≥ 20% of samples) across the three tissues. When considering the three tissues individually, we identified slightly more expressed genes in epididymis (20,376 genes) than in testis and vas deferens (20,222 and 19,051 expressed genes, respectively; Table 1). A majority of expressed genes were found in all three tissues (17,737 genes; Figure 1E) and were protein coding (87.4% – 89.7%; Tables S3). Testis had the most tissue-specific expressed genes (1,106 genes), followed by epididymis (443 genes), and vas deferens (227 genes; Figure 1E).

The cattle GTEx consortium analyzed 60 testis transcriptomes (Liu et al., 2022). However, most of them lacked metadata, were collected from pre-pubertal animals, or were individuals of non-taurine ancestry, precluding an immediate comparison with those from our homogeneous cohort. The abundance of 20,221 testis-expressed genes shared between ten cattle GTEx testis transcriptomes from post-pubertal (1.5 – 9 years) *Bos taurus taurus* bulls and our dataset was highly correlated (Pearson's r = 0.84). The correlation was higher (Pearson's r = 0.90) for 20,002 genes that were expressed with less than 500 TPM in our cohort. The expression of some genes differed between our cohort and the samples included in cattle GTEx (Figure S2), likely due to different RNA sequencing strategies applied to each dataset. The cattle GTEx dataset contained only one vas deferens and two epididymis transcriptomes from adult bulls of taurine ancestry, preventing a meaningful comparison with our data.

We used LeafCutter to detect RNA splicing variation and calculated 'percent spliced-in' (PSI) values for excised-intron clusters. Across the three tissues we observed 15,493 alternatively spliced genes, with 95% of these being protein-coding genes (14,719 genes; Table S3). We detected 11,087 genes that were alternatively spliced in all three tissues. Genes that were alternatively spliced in all three tissues were higher expressed than those for which we did not detect alternative isoforms (Table S4). We identified 139,186 splice junctions and 46,417 intron clusters in testis, 114,343 splice junctions and 44,891 intron clusters in epididymis, and 103,809 splice junctions and 40,480 intron clusters in vas deferens. The total number of genes with alternative splicing events was similar

across the three tissues, with 14,243, 13,558, and 12,332 alternatively spliced genes for testis, epididymis, and vas deferens, respectively.

The similarity of the transcriptional profile of the three male reproductive tissues was assessed through cluster analyses. Principal component analysis (PCA) of normalized expression values (TPM) and splicing phenotypes (PSI) separated samples by tissue type (Figure 1C; 1D), which was further supported by hierarchical clustering (Figure S3). In both expression and splicing PCAs, the first PC separated testis from epididymis and vas deferens, suggesting that the transcriptional profile of testis is distinct from other male reproductive tissues. To further explore the similarity between tissues, we inferred pairwise similarity of gene expression and splice-junction counts with Spearman correlation. For both expression and splicing, vas deferens and epididymis were more similar to each other than to testis (epididymis x vas deferens – expression: $\rho = 0.92$, splicing: $\rho = 0.83$; epididymis x testis – expression: $\rho = 0.82$, splicing: $\rho = 0.67$; vas deferens x testis – expression: $\rho = 0.74$, splicing: $\rho = 0.57$).

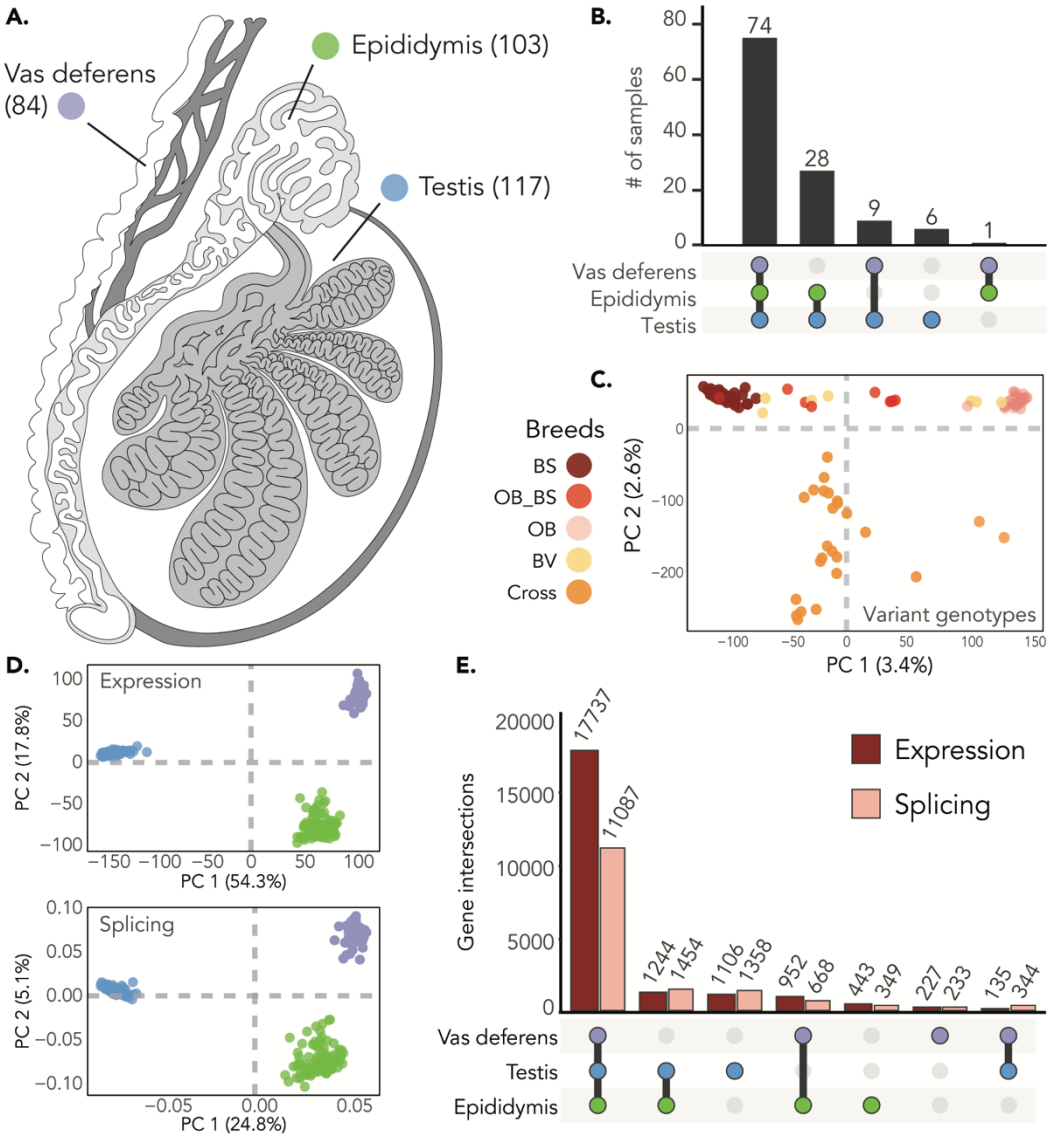

Figure 1. Overview of the molQTL cohort for three male reproductive tissues. A.) The three male reproductive tissues used in our study and the number of samples considered for each tissue. B.) Sample overlap across tissue types. Bar height represents the number of individuals. C.) PCA of LD-pruned sequence variant genotypes (366,090 variants total), with colors corresponding to the breed assigned by the Swiss Braunvieh herd book or "Cross". D.) Scatter plot of the top two principal components of PCAs of normalized expression values (TPM; top panel) and normalized splicing phenotypes (PSI; bottom panel) for all tissues. E). Overlap of expressed and spliced genes across the three tissues (based off the TPM and PSI matrices).

Thousands of variants impact gene expression and splicing

To identify loci that influence gene expression (expression QTL, hereafter referred to as eQTL), normalized and standardized TPM values were regressed on variants that had minor allele frequency greater than 1.0% and were within 1 Mb of the annotated transcription start site (TSS). We accounted for covariates such as age, RNA integrity, and hidden confounders that were estimated

directly from the data (PEER factors; Figure S4). We identified eQTL in at least one of the three tissues for 12,950 genes (hereafter referred to as eGenes) at a false discovery rate (FDR) of 5%. A majority of eGenes were protein-coding (11,951 eGenes; Table S3). Testis had considerably more eGenes than epididymis and vas deferens (Table 1)—over 55% of genes expressed in testis were also eGenes. Epididymis had 4,347 eGenes (21% of genes expressed in epididymis) and vas deferens had 3,889 eGenes (20% of genes expressed in vas deferens). One-third of testis eGenes had more than one independent-acting eQTL (Figure 2A), corresponding to 15,642 eQTL total and 3,687,265 unique significant variants (eVariants). We identified 4,768 independent eQTL (9.2% eGenes having > 1 eQTL; Figure 2A) and 925,916 eVariants in epididymis. Vas deferens had the fewest eQTL, with 4,211 independent eQTL and 673,696 eVariants. For all tissues, approximately half of all eQTL were within 100 kb of the TSS (8,000 testis eQTL; 2,802 epididymis eQTL; 2,423 vas deferens eQTL; Figure S5).

The effect of each eQTL was quantified as the allelic fold change (slope_aFC) in expression of the associated eGene. The slope_aFC value was highly correlated (Spearman's $\rho \geq 0.84$) with the beta coefficient from the linear model used for eQTL mapping (Figure 2B). Across the three tissues, only 2,321 eQTL (9.4%) had large effects (defined as $|\text{slope_aFC} \geq 1|$), with 65% of these loci residing within 100 kb of the eGene's TSS. Notably, testis had the smallest proportion of large effect eQTL (7.58%; 1,186 eQTL; Figure S5). The proportion of large effect eQTL in both epididymis and vas deferens was approximately 12% (599 and 536 eQTL in epididymis and vas deferens, respectively). We observed that eQTL annotated as non-coding transcript variants had a stronger effect on expression (median slope_aFC = 0.93; Figure 2D).

eQTL are expected to cause an imbalanced expression of the associated gene if they are cis-acting (Aguet et al., 2017; Pirinen et al., 2015). In this scenario, the expression of the associated eGene is influenced only by the linked eQTL allele leading to unbalanced expression of the eGene. Thus, to assess and independently quantify putative cis-regulatory effects of the eQTL, we investigated allelic imbalance in the expression of associated eGenes. In the three tissues between 78 and 80% of the variant-gene pairs were available to this evaluation, of which approximately a quarter (23 – 28%) showed significant evidence of allelic imbalance (FDR < 5%; Wilcoxon rank sum test). The proportion of eGenes that showed allelic imbalance was nearly twice as high (49.8, 46.8, and 47.2% in testis, epididymis, and vas deferens, respectively) for large effect eQTL ($|\text{slope_aFC}| \geq 1$; n = 1156, 669, 545 in testis, epididymis, and vas deferens, respectively (Figure S6B; Figure S6C)). Approximately three quarters (76.53, 76.53, and 74.49% for testis, epididymis, and vas deferens, respectively) of the eGenes with significant allelic imbalance were within 100 kb of the eQTL (Figure 2C). This is between

1.26- and 1.44-fold enrichment ($p < 2.16e-16$; Fisher's exact test) compared to random expectation (Figure S6A). The eQTL effect estimated as the magnitude of allelic imbalance (AI_aFC) was strongly correlated with slope_aFC (Spearman's $\rho = 0.69$, 0.73, 0.75 in testis, epididymis, and vas deferens, respectively). The correlation was even stronger (Spearman's $\rho = 0.87$, 0.88 and 0.88 for testis, epididymis and vas deferens, respectively) for a subset of the eQTL where the associated eGenes showed significant allelic imbalance (Figure S6C).

To identify variants that influence splicing, we conducted sQTL mapping between variants within 1 Mb of the intron cluster start site (ICSS) and intron-excision ratios of inferred intron clusters, which were normalized and standardized within and across samples, respectively. We identified 7,777 spliced genes across the three tissues with at least one sQTL (sGenes; Table 1) at an FDR of 5%—a majority of which were protein-coding genes (7,471 protein-coding genes; 96% of sGenes). Testis had the most sQTL of the three tissues, further corroborating its transcriptional complexity. We detected 7,000 sGenes in testis, which accounted for nearly half of its alternatively spliced genes. For epididymis and vas deferens, we identified 2,662 and 1,718 sGenes, respectively, corresponding to 20% and 14% of their spliced genes. In testis, 40.7% of sGenes had more than one independent-acting sQTL, resulting in 11,450 independent sQTL and 2,901,402 unique significant variants (sVariants; Figure 2A). Fewer sGenes had multiple independent-acting sQTL in epididymis and vas deferens (approximately 16% in epididymis and 11% in vas deferens; Figure 2A); in total, epididymis contained 3,165 sQTL and 683,747 sVariants while vas deferens contained 1,920 sQTL and 313,771 sVariants. In all tissues, between 60 and 70% of sQTL were located within 100 kb of the ICSS, corresponding to 6,822, 2,190, and 1,339 sQTL for testis, epididymis, and vas deferens, respectively (Figure 2E).

sQTL effects were quantified as the regression coefficient from the linear model used for sQTL mapping. There were few large effect sQTL (3,793 sQTL with $|\beta\text{-coefficient}| \geq 1$) across the three tissues. Most large effect sQTL were within 100 kb of the ICSS (65%, or 2,476 sQTL across all tissues; Figure 2E). The proportion of large effect sQTL was similar across the three tissues, corresponding to 22.7%, 22.5%, and 24.9% of sQTL in testis, epididymis, and vas deferens, respectively (2,603 sQTL in testis, 712 sQTL in epididymis, and 478 sQTL in vas deferens; Figure 2E). We observed that top sVariants within splicing regions—such as splice donor and splice acceptor sites—had the largest effect sizes (median effect size = 1.14; Figure 2F), corroborating that variants overlapping these nucleotides have pronounced impacts on pre-mRNA splicing.

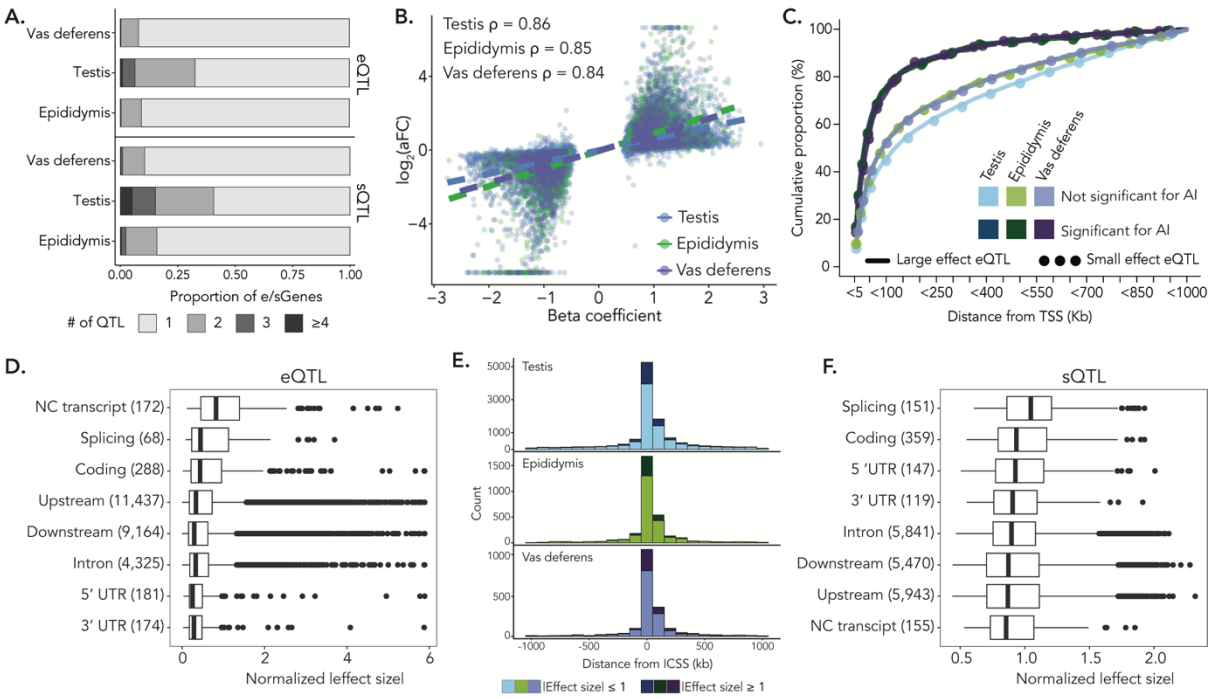

Figure 2. **Properties of eQTL and sQTL in three male reproductive tissues.** A.) Proportion of independent-acting eQTL (top) and sQTL (bottom) across tissues. B.) Correlation (Spearman's ρ) between the β-coefficient of the linear model (used for eQTL identification) and slope_aFC of each eQTL's top eVariant. The linear relationship between the two variables is shown with dotted lines. Colors correspond to the tissue type. C.) Cumulative proportion (%) of eQTL showing significant allelic imbalance in the expression of the associated eGene grouped (in bins of 5 Kb) by their proximity to the transcription start site (TSS). Data for large (|slope_aFC| ≥ 1) and small (|slope_aFC| < 1) effect eQTL are presented separately. Similar data for eQTL not showing significant allelic imbalance are shown for comparison D.) Annotation class of eQTL and rank-normalized absolute effect size for eQTL identified in all three tissues. The number of eQTL within an annotation class is listed in parentheses. E.) Distribution of sQTL (top independent-acting sVariants) from the ICSS for all three tissues. Darker colors represent large effect sQTL (|β-coefficient ≥ 1|). F.) Annotation class of sQTL and rank-normalized absolute effect size for sQTL identified in all three tissues. The number of sQTL within an annotation class is listed in parentheses.

Table 1. Results for e/sQTL mapping across tissues with a MAF filter of ≥ 1% and FDR of 5%.

	Testis	Epididymis	Vas deferens
Samples	117	103	84
Expressed genes	20,222	20,376	19,063
eQTL	15,642	4,768	4,211
eGenes	11,164	4,347	3,889
eGenes with >1 eQTL	3,647	402	310
eVariants	3,687,265	925,916	673,696
Spliced genes	14,243	13,558	12,332
sQTL	11,450	3,165	1,920
sGenes	7,000	2,662	1,718

sGenes with >1 sQTL	2,849	425	182
sVariants	2,901,402	683,747	313,771

Testis molQTL effects are unique and small, while molQTL effects in other male reproductive tissues are shared

Tissues with similar biological functions often share molQTL (GTEx Consortium, 2020; Liu et al., 2022; Urbut et al., 2019). Thus, we sought to determine if eQTL and sQTL in male reproductive tissues were shared or tissue-specific. We used Mashr to compare molQTL effects for genes that were expressed in all three tissues and considered 11,311 and 5,012 top eVariants and sVariants, respectively. For eQTL, we identified 10,738 variant-gene pairs that were significant in at least one tissue (local false sign rate (LFSR) < 0.05). A large proportion of eQTL were tissue-specific (4,760 eQTL; 44% of the eQTL considered), while there was a similar number of eQTL identified in either two or three tissues (two tissues: 2,949 eQTL, 27% of eQTL; three tissues: 3,029 eQTL, 28% of eQTL; Figure 3A). Testis had the most tissue-specific eQTL, followed by vas deferens, and epididymis (Figure 3B). eQTL effects were most similar between vas deferens and epididymis (Spearman's ρ = 0.58), and clearly less similar between testis and epididymis (Spearman's ρ = 0.32) and between testis and vas deferens (Spearman's ρ = 0.28). Conversely, most sQTL were ubiquitous—73% of the 4,737 variant-gene pairs were significant (LFSR < 0.05) in all tissues (3,451 sQTL; Figure 3A). Only 648 sQTL were tissue-specific (14% of sQTL considered; Figure 3A), most of which were in testis (505 sQTL; Figure 3B). We observed high pairwise similarity of sQTL effects across the three tissues, particularly between epididymis and vas deferens (testis x epididymis: Spearman's ρ = 0.75; testis x vas deferens: Spearman's ρ = 0.69; epididymis x vas deferens: Spearman's ρ = 0.88).

Tissue-specific molQTL typically have larger effects than those identified in many, or all, tissues (The FarmGTEx-PigGTEx Consortium et al., 2022; Urbut et al., 2019). We confirmed this phenomenon for epididymis- and vas deferens-specific eQTL, which had larger effects (slope_aFC) than eQTL found in all three tissues (vas deferens: Wilcoxon rank-sum p = 2.48e-16; epididymis: Wilcoxon rank-sum p = 0.003; Figure 3C). Vas deferens-specific sQTL also had larger effects than ubiquitous sQTL (Wilcoxon rank-sum p = 7.92e-11), though there was no statistical difference in sQTL effect size across tissue specificity classes for epididymis (Wilcoxon rank-sum p = 0.39). Alternatively, testis specific eQTL and sQTL had smaller effects than those shared across all three tissues (eQTL: Wilcoxon rank-sum p = 3.93e-30; sQTL: Wilcoxon rank-sum p = 1.40e-16; Figure 3D), suggesting that testis is composed of many tissue-specific small effect molQTL.

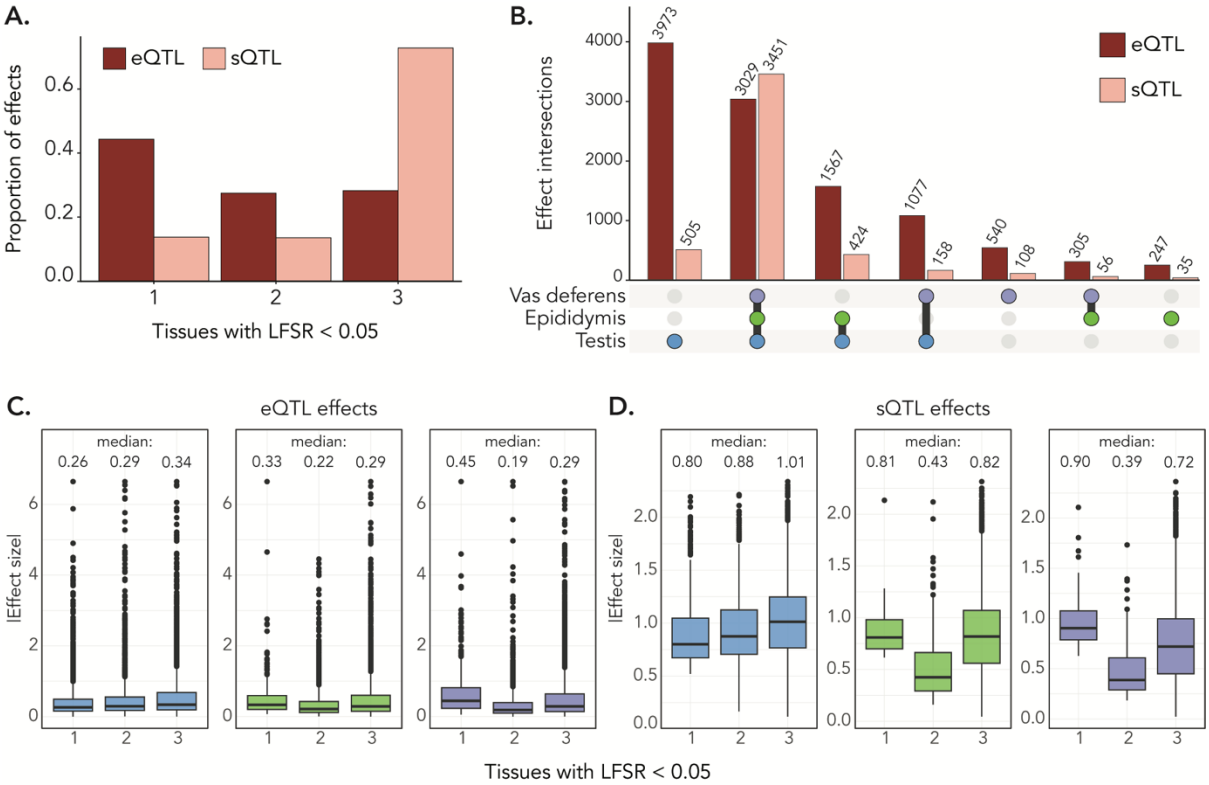

Figure 3. Tissue-specific and shared effects of eQTL and sQTL. A.) Proportion of eQTL and sQTL that are significant (LFSR < 0.05) in one, two, or three tissues. B.) Overlap of significant (LFSR < 0.05) eQTL and sQTL across the three tissues. Bar height represents the number of QTL. C.) Boxplots of the eQTL effect size across tissue specificity classes (significant in one, two, or all three tissues at a threshold of LFSR < 0.05) for testis (blue), epididymis (green), and vas deferens (purple) tissues. Absolute effect size corresponds to |aFC_slope|. Median effect size of each category is included. D.) Boxplots demonstrating the effect size of sQTL across tissue specificity classes for testis, epididymis, and vas deferens tissues. Absolute effect size corresponds to the β-coefficient of the linear model. Median effect size of each category is included.

Integration of molecular phenotypes, molQTL, and GWAS summary statistics reveals genes associated with male fertility

We sought to investigate the impact of molQTL on male reproductive ability. First, we conducted GWAS for male fertility with a cohort of 3,736 bulls that had imputed genotypes for 14,587,859 SNPs, and separately tested additive and non-additive inheritance. The fertility of the bulls was quantified through the proportion of successful artificial inseminations and accounted for genetic and environmental factors (see Hiltpold et al., 2021). While the GWAS cohort had no overlap with the molQTL cohort, both predominantly consisted of Brown Swiss bulls. Non-additive association testing revealed four male fertility QTL on chromosomes 1, 6, 18, and 26 (significance threshold of 5e-08) that contained 4,890 variants (Figure 4A). Additive GWAS did not detect any additional

significant associations and failed to identify the QTL on chromosomes 1 and 18. The QTL on chromosomes 6 and 26 were detected by the additive GWAS, but with lower significance (Figure S7).

We implemented the MetaXcan framework to establish if variation in molecular phenotypes is associated with variation in male fertility. Briefly, S-PrediXcan was used to integrate summary statistics from the non-additive GWAS with expression and splicing phenotypes from the three reproductive tissues. Signals were subsequently filtered based on the colocalization probability between male fertility QTL and molQTL. We identified two and seven unique genes for expression and splicing, respectively, that overlapped three of the male fertility QTL (Figure 4, Table 2). The most striking association was on chromosome 6; *WDR19* encoding WD Repeat Domain 19 was the most significantly associated gene in epididymis and vas deferens (p = 3.17e-43 and 1.04e-48). An intron cluster encompassing a canonical (58373894:58374821) and a cryptic (58373885:58374821) splice junction was the top fertility-associated molecular phenotype in both tissues (Figure S8). A highly significant S-PrediXcan signal (p = 6.10e-38) was also obtained for this *WDR19* intron cluster in testis, however the evidence for colocalization with the GWAS peak was low (PP.H4.abf = 0.39).

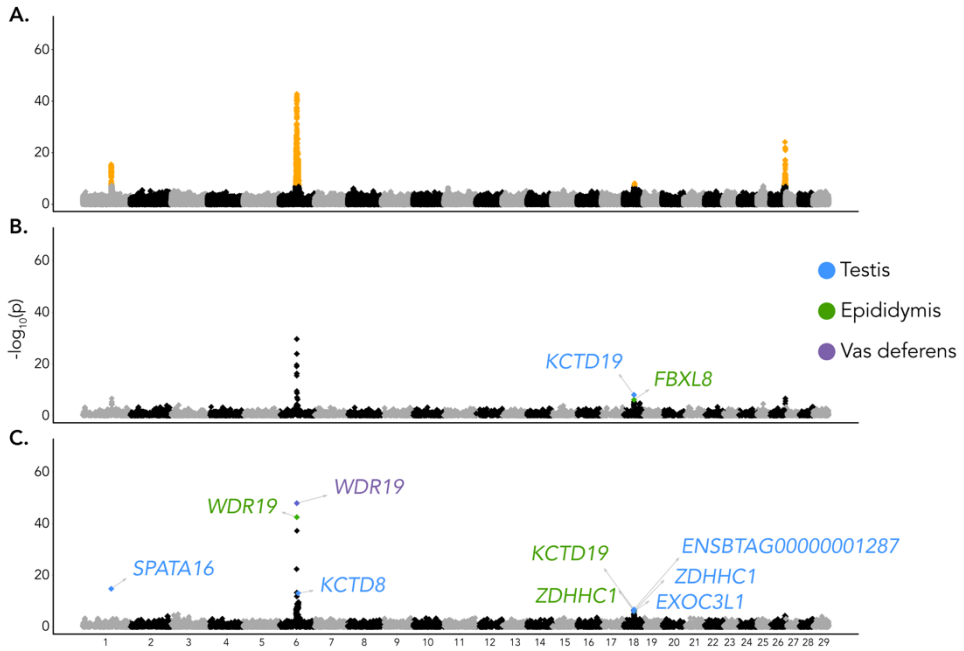

Figure 4. Genes associated with male fertility. Manhattan plots showing genome-wide association between (A) male fertility and imputed sequence variants from non-additive association models. Variants significantly (p < 5e-8) associated with male fertility are highlighted in orange. Transcriptome-wide association with S-PrediXcan between (B) expression values or (C) splicing phenotypes and male fertility. Significantly associated genes after the stringent filtering based on the MetaXcan framework are marked with their names.

The splicing MetaXcan in testis revealed an association (p = 1.71e-15) between *SPATA16* encoding spermatogenesis associated protein 16 and male fertility (Figure 4C). *SPATA16* mRNA was highly expressed in testis (270.57 ± 32.26 TPM), lowly expressed in epididymis (15.28 ± 9.90 TPM), and barely expressed in vas deferens (1.05 ± 1.18 TPM). Only one *SPATA16* transcript is annotated in Ensembl, but the Refseq annotation suggests three isoforms, of which the canonical isoform (XM_002684936.6) was 12 and 17 times more abundant in testis than two alternative isoforms XM_024995427.1 and XM_005201702.4 (Figure S9A). The fertility-associated *SPATA16* intron cluster comprised four splice junctions that span the first four exons, including a non-coding exon that is only part of the Refseq annotation (Figure 5C; Figure 5D; Figure 5F). The fertility and splicing QTL were colocalized with a probability of 0.86 and a variant (Chr1:93,954,637 bp) 365 kb upstream the annotated *SPATA16* transcription start site was the most probable causal variant (Figure 5A). An association analysis conditional on Chr1:93,954,637 did not identify any additional variants as being associated with male fertility on chromosome 1 (Figure 5B).

The Chr1:93,954,637 T allele compromises male fertility (p = 4.15e-16; Figure 5E) but is associated with increased *SPATA16* mRNA expression (β = 0.71 ± 0.17 TPM_{norm}; p = 6.41e-05)—albeit not at the stringent significance threshold applied to our eQTL analysis (Figure S9B; Figure S9C). Eleven of the twelve *SPATA16* exons were expressed at higher levels in animals carrying the T allele, though this difference was only significant (p = 3.7e-06) for the fourth exon (94,396,748 bp – 94,396,893 bp). Interestingly, the second exon (94,323,018 bp – 94,323,140 bp) is the only exon for which abundance is reduced (β = 0.25 ± 0.09 TPM_{norm}; p = 0.0057) by the Chr1:93,954,637 T allele (Figure S9E). This exon is part of SPATA16 isoform XM_024995427.1 but is absent in both the canonical (XM_002684936.6) and another alternative isoform (XM_005201702.4). While the Chr1:93,954,637 T allele has no effect on the abundance of the predominant canonical isoform (XM_002684936.6, p = 0.15), it increases (β = 3.6 ± 0.68 TPM; p = 6.7e−07) abundance of XM_005201702.4 and reduces abundance of XM_024995427.1 (β = −1.1 ± 0.42 TPM; p = 0.015), suggesting that it promotes differential isoform usage (Figure S9D). This is further supported by an inverse association between inclusion ratios of the second and third exon with the abundance of two alternative SPATA16 isoforms (XM_005201702.4 and XM_024995427.1; Figure S10).

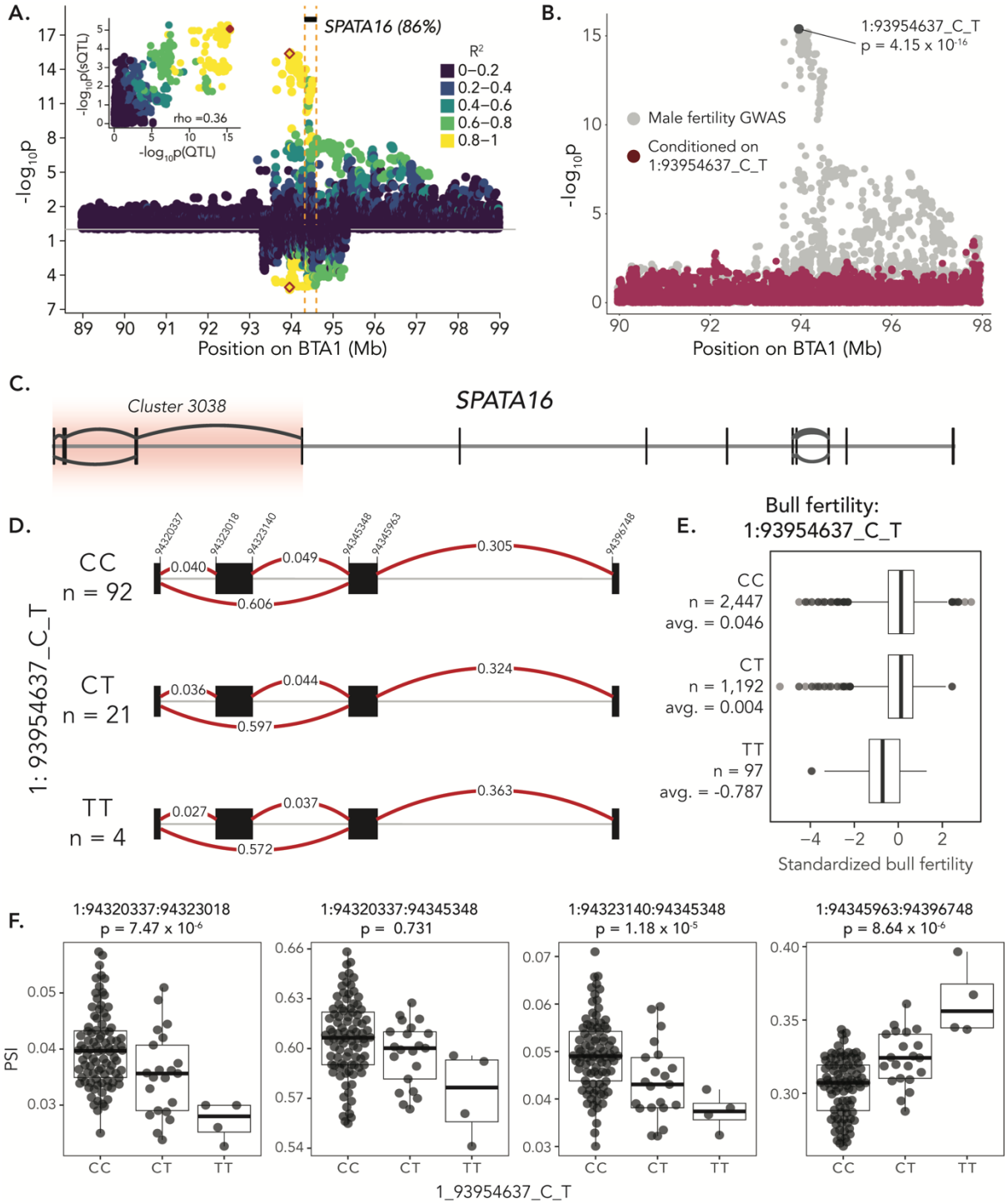

Figure 5. A molecular *SPATA16* phenotype overlaps with a male fertility QTL. A.) Mirrored plots of $-\log_{10}$(p)-values from association testing between imputed sequence variants and bull fertility (top) and splicing phenotypes for intron cluster 3038 of the gene *SPATA16* (bottom). The inset shows the correlation between GWAS and sQTL $-\log_{10}$(p)-values. Color indicates the linkage disequilibrium (R^2) between the most likely colocalized variant (1:93954637_C_T, red colored) and all other variants. B.) Association testing between imputed sequence variants and male fertility before (gray) and after (maroon) conditioning on the genotype of the most likely colocalized variant (1:93954637_C_T). C.) Gene structure of bovine *SPATA16*, showing positions of exons (black lines) and alternative splicing events (arcs). D.) Splicing within *SPATA16* intron cluster 3038 for

different genotypes of the top colocalized variant. Red lines show the different splice junctions with the values representing "percent spliced in" estimates within the intron cluster. E.) Standardized bull fertility across the genotypes of the colocalized variant. F.) PSI values for different splicing events within Cluster 3038 across different genotypes of the most likely colocalized variant.

The non-additive GWAS for male fertility revealed a QTL on chromosome 18 (p = 6.41e-09, lead SNP at 36,480,384) that coincides with a previously localized 3 Mb region (between 34 and 37 Mb), for which no compelling candidate causal variants were found (Hiltpold et al., 2021). This 3 Mb window contains 97, 27, and 12 eQTL and sQTL in testis, epididymis and vas deferens, respectively. The MetaXcan and colocalization analyses revealed five significantly associated genes (*ENSBTAG00000001287*, *EXOC3L1*, *FBXL8*, *KCTD19*, *ZDHHC1*) at this QTL, of which *KCTD19* encoding the potassium channel tetramerization domain containing protein 19 shows a highly testis-biased expression (Table 2). Two genes (*KCTD19* and *ZDHHC1* encoding the zinc finger DHHC-type containing protein 1) were each associated with two molecular phenotypes in two tissues. Three variants (Chr18:34,914,479, Chr18:34,815,920, Chr18:35,059,627), which are in moderate LD (between 0.54 and 0.6), are colocalized for the male fertility QTL and seven distinct molecular phenotypes (Table 2). Association analyses conditional on any of these variants did not identify additional variants associated with male fertility on chromosome 18. The Chr18:34,914,479 T allele is associated with higher fertility, an increased KCTD19 mRNA abundance in testis, and the expression of a KCTD19 isoform in the epididymis that has an additional 30 bp coding sequence added to the 14th exon which results in a protein that is 10 amino acids longer than that encoded by the canonical form (Figure S11). Alternative *KCTD19* splicing was also highly significant (p = 3.13e–15) in testis, but MetaXcan did not reveal association of this molecular phenotype with male fertility. This variant (Chr18:34,914,479) was also associated with differential *ZDHHC1* splicing in epididymis and differential *EXOC3L1* splicing in testis.

A QTL (p = 7.59e-23, lead SNP at Chr26:50,145,932) for male fertility was detected on chromosome 26. Neither the splicing nor the expression MetaXcan revealed any significant gene-trait associations for this QTL.

Table 2. Male fertility-associated genes prioritized by MetaXcan. P-value is the gene's p-value from S-PrediXcan. PP.H4 is the probability of a shared causal variant for molQTL and QTL from colocalization analysis. Colocalized variant is the most likely colocalized variant from coloc.abf (H4.PP.SNP with largest posterior probability). β–coefficient is the effect estimate of the most likely colocalized variant from the linear model used for molQTL mapping.

Gene	Expression (TPM)			Splice junction and intron cluster	Molecular phenotype	Tissue	P-value	PP.H4	Colocalized variant	β–coefficient
	Testis	Epididymis	Vas deferens							
SPATA16	270.57 ± 32.26	15.28 ± 9.90	1.05 ± 1.18	1:94345963-94396748:clu_3038	Splicing	Testis	1.71 E-15	0.86	Chr1: 93,954,637	0.78
WDR19	20.09 ± 2.65	29.46 ± 19.57	36.26 ± 4.82	6:58373894-58374821:clu_63814	Splicing	Epididymis	3.17 E-43	0.96	Chr6: 57,900,948	-1.17
				6:58373894-58374821:clu_46646		Vas deferens	1.04 E-48	0.99	Chr6: 57,900,948	-1.34
KCTD8	2.71 ± 0.73	0.73 ± 1.00	0.68 ± 0.93	6:62885148-62886027:clu_81370	Splicing	Testis	8.10 E-14	0.81	Chr6: 62,206,554	-0.73
KCTD19	238.01 ± 56.20	9.05 ± 6.26	0.58 ± 1.42	--	Expression	Testis	2.27 E-07	0.96	Chr18: 34,914,479	1.12
				18:34910787-34910930:clu_25862	Splicing	Epididymis	2.28 E-07	0.87	Chr18: 34,914,479	0.67
ZDHHC1	21.96 ± 3.04	24.77 ± 17.29	21.00 ± 3.32	18:35019435-35026730:clu_33937	Splicing	Testis	8.11 E-07	0.94	Chr18:34,815,920	-1.12
				18:35019435-35026730:clu_25875		Epididymis	9.44 E-07	0.92	Chr18: 34,914,479	-0.81
FBXL8	3.80 ± 1.51	2.05 ± 0.72	1.52 ± 0.46	--	Expression	Epididymis	7.86 E-07	0.87	Chr18:35,059,627	0.96
EXOC3L1	13.50 ± 2.15	1.34 ± 0.55	1.73 ± 0.50	18:34825696-34825972:clu_33908	Splicing	Testis	9.91 E-07	0.93	Chr18: 34,914,479	0.87
ENSBTAG00000001287	7.17 ± 0.97	3.33 ± 1.00	3.26 ± 0.81	18:34842264-34842709:clu_33910	Splicing	Testis	1.73 E-07	0.93	Chr18: 34,815,920	-0.91

Discussion

We characterized the transcriptomic profile of testis, epididymis, and vas deferens in a cohort of 118 bulls. To the best of our knowledge, a cohort of this size has not been established for male reproductive tissues for any species. Our molQTL cohort contained bulls within a narrow post-pubertal age range that predominantly belonged to one taurine breed. We demonstrated the benefit of establishing such a homogeneous cohort for transcriptome analyses, as we detected 14-times (11,164 vs. 809) more eGenes and 7-times more sGenes (11,450 vs. 1,573) in testis than cattle GTEx (Liu et al., 2022) despite our molQTL cohort being only twice as large (117 individuals vs. 60 individuals in cattle GTEx). This suggests that the heterogeneity of cattle GTEx likely leads to substantial underestimation of the transcriptional complexity of bovine testis. The number of

eGenes and sGenes identified in our study is similar to what was reported in a heterogeneous—but three-times larger—human GTEx cohort (GTEx Consortium, 2020), thus providing a valuable resource for translational research in mammalian male reproductive biology. Comparing our findings with similar-sized cohorts sampled at other developmental stages will reveal spatiotemporal transcriptomic changes in male reproductive tissue, such as those occurring during testicular development and puberty (Guo et al., 2020; Liu et al., 2023).

Our comprehensive set of expressed and spliced genes enabled us to thoroughly characterize the transcriptional complexity of three reproductive tissues. We revealed nearly 20,000 expressed and 14,000 spliced genes within each tissue. Expressed and spliced genes were generally shared across the three reproductive tissues; however, the transcriptional profiles of vas deferens and epididymis were similar, while that of testis was distinct. We observed a similar pattern for eQTL and sQTL—the effects of regulatory variants in vas deferens and epididymis were similar and often shared, whereas testis had a distinct and exceptionally large array of eQTL and sQTL. When compared to the other tissues, we found between 3- and 6-times the number of eGenes and sGenes in testis, many of which were regulated by multiple eQTL and sQTL, respectively, which emphasizes its transcriptional complexity that has been reported previously (Ramsköld et al., 2009; Soumillon et al., 2013). Testis contained thousands of tissue-specific, small effect molQTL. An abundance of molQTL in testis was observed in numerous mammalian species (GTEx Consortium, 2020; The FarmGTEx-PigGTEx Consortium et al., 2022), though the reason for this remains unclear. The accumulation of small effect molQTL in testis may be a result of male sexual selection and sperm competition, which is driven by a more permissive transcription (Soumillon et al., 2013), relaxed pleiotropic constraints, and other selective mechanisms (Kaessmann, 2010; Murat et al., 2023). In humans, when compared to other tissues, testis eQTL were more likely to contain signatures of positive selection (Quiver & Lachance, 2022); furthermore, tissue specific eQTL that showed evidence of positive selection had small effect sizes (Quiver & Lachance, 2022). Thus, functional variants in testis may experience unique selection pressures that are essential for male reproduction. Further research is warranted to fully understand the genomic basis of testis's complex functional patterns.

By leveraging our comprehensive array of molecular phenotypes from reproductive tissues and fertility records from genotyped artificial insemination bulls through gene-based association testing and colocalization analyses, we identified candidate causal regulatory mechanisms underpinning three of the four male fertility QTL. Among them is a previously suspected candidate causal molecular phenotype of *WDR19* (Hiltpold et al., 2020), which adds additional confidence that this

approach provides biologically meaningful associations. Our results corroborate that gene splicing and expression variation have substantial effects on complex traits (Xiang et al., 2022) and highlight that regulatory variants need to be considered thoroughly as candidate causal variants. The male fertility QTL were associated with two large effect and one small effect molQTL, thereby demonstrating that molQTL effect size may be a poor predictor of impact on complex trait variation. Spermatogenesis, sperm maturation, and sperm transport are pivotal functions of the three reproductive tissues considered. Gene-based association testing with traits such as sperm morphology or sperm motility may reveal additional gene-trait associations, as they are closer related to the biological function of these tissues than male fertility. However, establishing cohorts with repeated semen quality measurements that are large enough to identify loci that explain only a small proportion of trait variation is challenging in cattle—and almost impossible in most other species.

We also identified an alternative splicing event in testis for *SPATA16* that was significantly associated with male fertility. The colocalized variant fell within an intergenic region between *SPATA16* and *NLGN1*. Previously, a GWAS-only approach prioritized a missense variant of *SPATA16* as a putative causal variant (Hiltpold et al., 2021). However, by combining molecular phenotypes, molQTL analyses, and GWAS—which were appropriately modeled to QTL inheritance—we identified an alternative splicing and regulatory mechanism that is significantly more likely to underpin the QTL. While loss-of-function alleles of *SPATA16* lead to severe sperm defects that prevented fertilization (Dam et al., 2007; Fujihara et al., 2017), our results demonstrate that variants mediating *SPATA16* expression and splicing can contribute to quantitative variation in male fertility as they are less deleterious to protein function. We also identified several gene-trait associations that showed colocalization between molQTL and a non-additive male fertility QTL on chromosome 18. Our inability to resolve this QTL may be due to high linkage disequilibrium or possibly indicates that the causal variant affects multiple genes, as may be the case for large structural variants (Leonard, Crysnanto, et al., 2023). While we were unable to conclusively identify the molecular underpinnings of this male fertility QTL with our integrative approach, MetaXcan prioritized genes that were previously implicated in male fertility disorders, including *KCTD19* and *ZDHHC1* (Oura et al., 2021; S. Wang et al., 2021; W. Wang et al., 2023). Thus, future fine-mapping efforts that consider additional phenotypic observations and complex genotype variations, such as structural variants called from long read cohorts, will be required to fully describe the molecular underpinnings of this QTL (Leonard, Mapel, et al., 2023).

Methods

Ethics statement

Tissue was sampled at a commercial abattoir. The decision to slaughter the bulls was independent from our study. None of the authors of the present study were involved in the decision to slaughter the bulls. No ethics approval was required for this study.

Tissue sampling and DNA/RNA extraction

Testes from 128 bulls were collected at a commercial abattoir in Zürich, Switzerland after regular slaughter, then transported to a laboratory for preparation. Testis, epididymis (caput), and vas deferens tissue samples were flash-frozen in liquid nitrogen and stored at -80°C until DNA and RNA extraction. The time from slaughter to freezing ranged from 40 minutes to 270 minutes (average: 126 minutes ± 47 minutes). Sample collection took place during the fall, winter, and spring of 2019, 2020, and 2021. Breed was assigned according to entries from the Swiss Braunvieh herdbook and the animal traffic database.

We extracted DNA and total RNA from testis tissue with Qiagen AllPrep Mini kits (Qiagen, Hilden, Germany). Frozen testis tissue was homogenized with a MagNA Lyser (Roche, Basel, Switzerland) at 6000 rpm for 50 seconds (x2) in RTL Plus Buffer with β-mercaptoethanol. DNA extraction followed standard manufacturer protocols. Concentration was estimated with a Qubit 2.0 fluorometer (Thermo Fisher Scientific) prior to submission for whole genome sequencing (WGS). Extraction of testis total RNA followed manufacturer protocols. Epididymis and vas deferens total RNA was extracted from frozen tissue with Qiagen RNeasy Mini Kits (Qiagen, Hilden, Germany) and included an on-column DNase digestion with Qiagen RNase-Free DNase (Qiagen, Hilden, Germany). Frozen epididymis tissue was homogenized with the same conditions as described for testis tissue. We optimized the homogenization and lysis of vas deferens tissue by adding an additional homogenization period at 6000rpm for 50 seconds and a 60-minute waiting period. We assessed the quality of testis, epididymis, and vas deferens total RNA with an RNA integrity number (RIN) inferred from a Bioanalyzer RNA 600 Nano assay (Agilent Technologies). For subsequent analyses, we only considered samples with RIN > 4.0.

DNA and RNA sequencing

Genomic libraries (paired-end, 150 bp) for WGS were prepared with the Illumina TruSeq DNA PCR-Free protocol and sequenced on two Illumina NovaSeq 6000 S4 flowcells. Paired-end total RNA libraries (150 bp) were prepared with the TruSeq Stranded Total RNA protocol and included rRNA depletion with Ribo-Zero Plus. Libraries were sequenced on four S4 flowcells and one S2 flowcell of the Illumina Novaseq 6000.

DNA alignment and variant calling

We used fastp (v0.19.4; Chen et al., 2018) with default parameters to remove adapter sequences and low-quality bases, and trim poly-G tails from raw DNA sequence data. After quality control, we aligned reads to the ARS-UCD1.2 reference genome (Rosen et al., 2020) with the mem-algorithm from BWA (v0.717; H. Li, 2013) and the -M flag. We sorted the aligned reads by coordinates with Sambamba (v0.6.6; Tarasov et al., 2015), then combined the read-group specific BAM files to create sample-specific sorted BAM files. We marked duplicate reads in the sample specific sorted BAM files with the MarkDuplicates module from Picard tools (https://broadinstitute.github.io/picard/). We used mosdepth (v0.6.6; Pedersen & Quinlan, 2018) to infer the sequencing coverage at a given genomic position, which was then used to estimate the average coverage per sample. Only high-quality reads (mapping quality > 10 or without SAM flag 1796) were considered when calculating the average coverage. We called variants with DeepVariant (v1.3; (Poplin et al., 2018) using the WGS mode. Called samples were merged using GLnexus (v1.4.1; Yun et al., 2020) with the "DeepVariantWGS" configuration. Variants that had a missingness rate greater than 50% and variants for which the genotypes deviated from Hardy-Weinberg proportions (P < 1e-08) were removed. We applied Beagle (v4.1; Browning & Browning, 2016) to impute sporadically missing genotypes and infer haplotypes, then removed sites with model-based imputation accuracy < 0.5. To assess relationships among individuals, we constructed a genomic relationship matrix with 366,090 LD-pruned variants (obtained from Plink v1.9 with --indep-pairwise 1000 5 0.2; Chang et al., 2015) that had MAF > 0.5% and performed a PCA with the "pca" function in QTLtools (Delaneau et al., 2017).

RNA alignment

We removed adapter sequences, low-quality bases, poly-A tails, and poly-G tails from the RNA sequence data with fastp. We split cleaned reads into read groups with gdc-fastq-splitter (https://github.com/kmhernan/gdc-fastq-splitter) then aligned them to the cattle reference genome (ARS-UCD1.2) and the Ensembl gene annotation (release 104) with STAR (version 2.7.9a; Dobin et al.,

2013). To account for allelic mapping bias in the sQTL and allele specific expression (ASE) analyses, we produced additional alignments with the flag --waspOutputMode and heterozygous SNPs. We performed coordinate sorting and added read groups with Picard (https://broadinstitute.github.io/picard/). We merged each sample's BAM files with Sambamba (v0.6.6; Tarasov et al., 2015) and marked duplicate reads with the MarkDuplicates module from Picard (https://broadinstitute.github.io/picard/). Statistics on the alignment quality were inferred with the flagstat function from Sambamba for each sample.

Expression and splicing quantification

We quantified gene-level expression with the "quan" function in QTLtools. We produced gene-level TPM values with high quality reads that passed all alignment quality filters and only included reads that were uniquely mapped and properly paired. Gene-level read counts were inferred with featureCounts (Liao et al., 2014). We filtered expression values for each tissue to include genes with expression ≥ 0.1 TPM and ≥ 6 reads in ≥ 20% of samples. The filtered expressed genes were inverse normal transformed and quantile normalized for subsequent analyses (Robinson & Oshlack, 2010). To observe clustering within and across tissue types, we used the filtered, normalized TPM values to perform a PCA and hierarchical clustering with the dendextend (v1.16.0) package in R.

To infer splicing events, we quantified intron-excision values for identified intron clusters. We extracted exon-exon junctions from reads that passed WASP filtering with Regtools (Cotto et al., 2023) and considered a minimum anchor length of 8 bp, minimum intron size of 50 bp, and maximum intron size of 500,000 bp. Intron clustering, calculation of intron excision ratios, filtering, and preparation for sQTL mapping was performed with Leafcutter (Y. I. Li et al., 2018) and executed with the cluster_prepare_fastqtl.py wrapper provided by the human GTEx consortium (https://github.com/broadinstitute/gtex-pipeline/tree/master/qtl/leafcutter). We assigned clusters to annotated genes with an altered map_clusters_to_genes.R script that accounted for strandedness and gene coordinates from a collapsed gene annotation for cattle (Ensembl release 104; generated with scripts from https://github.com/broadinstitute/gtex-pipeline/tree/master/gene_model). We limited our dataset to high-quality introns by imposing stringent filters that removed introns without read counts in > 50% of samples, introns with low variability across samples, and introns with fewer than max (10, 0.1n) unique values (where n is sample size). To normalize the filtered counts and produce files for sQTL mapping, we used the prepare_phenotype_table.py script from Leafcutter.

We performed hierarchical clustering and conducted a PCA on the resulting normalized intron excision phenotypes and hierarchical clustering with the dendextend package in R.

eQTL mapping, allelic imbalance, and sQTL mapping

eQTL mapping was performed for all three tissues with QTLtools. To account for population structure and other covariates that influence gene expression, normalized expression phenotypes were corrected with the first three genotype PCs, ten PEER (Stegle et al., 2012) factors (estimated for each tissue of interest; Figure S4), the age of the individual, and RIN value of the sample. We considered sequence variants with MAF > 1% and included variants 1 Mb up- and downstream of the transcription start site (TSS). To account for multiple testing, we used the "permute" function in QTLtools to conduct 1000 permutations and produce beta corrected p-values. We used the adjusted p-values and the qtltools_runFDR_cis.R script to apply a false discovery rate (FDR) threshold of 5% and identify expressed genes with at least one significant eQTL. To identify all significant variant-gene pairs, we followed the procedure detailed in Delaneau et al., (2017). Specifically, each gene's beta p-values and most-likely beta parameters were used with the FDR level to feed the beta quantile function. This generated nominal p-value thresholds for each expressed gene, and all variants below this threshold were deemed significant. To identify genes with multiple independent acting eQTL, we implemented the conditional analysis from QTLtools. Briefly, this process uses the aforementioned nominal p-value thresholds to identify all significant eVariants, then implements forward and backward stepwise linear regression to identify independent acting eQTL. The significant eVariants are then assigned to the independent signals.

To estimate the effect size of significant eQTL, we computed the log allelic fold change (slope_aFC; Mohammadi et al., 2017) with aFC.py (https://github.com/secastel/aFC) for the top variant of each independent eQTL. We used gene counts from featureCounts, which were normalized with DESeq2 (Love et al., 2014) and log transformed. We compared the normalized eQTL effect sizes to the annotation category of the top variant (obtained with the Variant Effect Predictor (VEP) from Ensembl; McLaren et al., 2016 et al., 2016) to investigate functional consequences.

We studied allelic imbalance using RNA sequencing reads filtered with WASP (Van De Geijn et al., 2015) to mitigate reference allele bias. Whole genome DNA sequence data phased with beagle 5.4 (Browning et al., 2021) were complemented with the "read backed phasing" of the RNA seq data using phASER (Castel et al., 2016) with the flag --baseq 10. Sequencing reads overlapping

heterozygous sites within protein coding genes (Ensembl version 104) were used to produce gene level haplotypic expression counts using phASER_gene_AE.py with the –min_haplo_maf 0.005 flag. A median number of 3,834, 3,345, and 1,353 RNA sequencing reads per gene, and 6,352,369, 8,453,661 and 6,739,602 reads per sample covering the heterozygous sites of the protein coding genes were available in testis, epididymis, and vas deferens, respectively. Haplotype expression counts across all samples were compiled using phaser_expr_matrix.py to validate cis-regulatory effects of eQTL identified in the three tissues and to independently estimate their effects. eGenes harboring heterozygous sites covered with at least 8 sequencing reads and top eVariants with at least 10 homozygous and 10 heterozygous individuals were considered for this assessment, resulting in a subset of 12,261, 3,832, and 2,871 variant-gene pairs in testis, epididymis, and vas deferens, respectively. Gene level haplotypes were then phased with their associated top eVariant using phaser_cis_var.py. Individual level magnitude of allelic imbalance was estimated as log allelic fold change (AI_aFC) using phaser_cis_var.py. The AI_aFC is the ratio of gene haplotype counts linked to alternative allele to the gene haplotype counts linked to the reference allele of the top eVariant on log2 scale. The median of AI_aFC in individuals heterozygous for the top eVariant is presented as an independent estimate of the cis regulatory effect of that eQTL. Comparison of AI_aFCs in individuals heterozygous for the top eVariant allelic imbalance expected) and homozygous for the top eVariant (allelic imbalance not expected) was used to test the significance of allelic imbalance using a Wilcoxon ranksum test implemented in phaser_cis_var.py.

sQTL mapping was performed with QTLtools and generally followed the approach used for eQTL discovery. However, we used the “grp-best” option to adjust the permutation scheme to correct for multiple splice junctions and intron clusters within a gene. Mapping was conducted with variants 1 Mb up and downstream of the TSS and we included three genotype PCs, age, RIN, and ten PEER factors as covariates. We conducted the QTLtools conditional analysis to identify all significant variants (sVariants) and independent acting sQTL. We considered the β–coefficient from the QTLtools linear model for the top sVariant as the sQTL effect size. Normalized sQTL effect sizes were compared across VEP functional annotation categories using the previously described variant annotation classes.

Shared eQTL and sQTL

We identified shared and tissue specific QTL with Mashr (v0.2.69; Urbut et al., 2019). We included top eVariants and sVariants from genes that were expressed in all three tissues. To prevent the double-counting of molQTL that are in linkage disequilibrium and impact the same gene or intron

cluster, we selected a single top molQTL that had the largest effect across tissues (as described in Urbut et al., 2019). This resulted in 11,311 eVariants and 5,012 sVariants. We considered a subset of 200,000 randomly selected variants and invoked a threshold of LFSR < 0.05 to establish if an effect was significant in a tissue. For significant effects, we assessed pairwise tissue similarity with Spearman's correlation. We compared the magnitude of molQTL effect sizes across specificity classes (tissue specific, in two tissues, or in all tissues) for each tissue with a Wilcoxon signed rank test.

GWAS of male fertility

Genome-wide association tests assuming additive and non-additive modes of inheritance were carried out between imputed genotypes and estimates of sire insemination success (which we used as a proxy for "male fertility"; Hiltpold et al., 2021) in 3,736 bulls using GCTA (Yang et al., 2011). The additive association testing was carried out using additively coded SNP genotypes. For the non-additive association testing, SNP genotypes were coded assuming recessive inheritance to the reference (R) allele and alternate (A) allele. Genotypes were coded as RR = 1, RA = 0, AA = 0 (M1) in the former case and as AA = 1, RA = 0, RR = 0 (M2) in the latter case. Only SNPs with MAF > 0.5% and where the frequency of 1's was between 0.5% and 0.95% (N = 14,587,856) were retained for association testing. The smallest P value from M1 and M2 was considered as the strength of non-additive association between genotypes and phenotypes for each of the tested variant, and variants with P < 5e-08 were considered significant. A genomic relationship matrix constructed from 18,187,234 autosomal SNPs with MAF > 0.005 was included in the association model to control for relatedness among samples.

Integrating QTL and molQTL in MetaXcan framework

We used S-PrediXcan (Barbeira et al., 2018) to test for an association between molecular phenotypes (expression and splicing phenotypes) and male fertility. The summary statistic-based approach was applied to include results from non-additive association testing. Briefly, we trained elastic-net based prediction models for expression values (TPM) and splicing phenotypes (PSI), respectively, for all genes and intronic clusters separately in testis, epididymis, and vas deferens. SNPs located within 1 Mb of the TSS of the genes were considered for training with the script gtex_tiss_chrom_training.R. In total, 18,053,560 sequence variants (MAF > 1%) called in the molQTL cohort were available for training the prediction models. Covariates used in the eQTL and sQTL scans were included in training of respective prediction models to account for confounding factors. High-performance prediction models (zscore_pval < 0.05 and rho_avg > 0.1) were available to predict

expression levels of 15,810 genes and to predict splicing phenotypes for 46,426 intron clusters across three tissues (77, 80, and 58% of eGenes and for 92, 94, and 80% of intron clusters in testis, epididymis, and vas deferens respectively). Using weights for each SNPs in these high-performance prediction models, we then carried out gene level and cluster level association test for expression and splicing phenotype respectively using the script SPrediXcan.py. Following the recommendations in Barbeira et al., (2018), Bonferroni-corrected P values of 3.16e-06 (0.05/15,810) and 1.08e-06 (0.05/46,426), respectively considering the number of genes and intron clusters tested for expression and splicing phenotypes, were set as a significant threshold. Further, a filter was applied on the prediction performance of the model with the threshold set at 0.05/number of significant results after the previous filtering.

Next, to avoid capturing LD-contaminated associations, as recommended in the MetaXcan framework (Barbeira et al., 2018), we carried out Bayes Factor colocalization analyses with the R package coloc (Giambartolomei et al., 2014). For every significant GWAS signal ($p < 5e-08$), we searched for evidence of its colocalization with molQTL using the “coloc.abf” function. The search space was limited to 5 Mb up- and downstream of the significant GWAS peaks. Colocalizations with PP.H4.abf (probability of a shared causal variant) > 0.8 and PP.H3.abf (probability of different causal variants) < 0.5 were retained and used to filter TWAS results.

Characterization of a SPATA16 sQTL

The Ensembl annotation of *SPATA16* contains only one transcript, whereas the Refseq annotation suggests three isoforms (XM_002684936.6, XM_024995427.1, XM_005201702.4) that differ in both the number of coding and the number of non-coding exons. The abundance of the three isoforms was quantified with kallisto (Bray et al., 2016). Testis RNA sequencing data was processed and aligned to the cattle reference genome (ARS-UCD1.2) and the Refseq gene annotation (version 106) with STAR (see above). Exon-specific SPATA16 expression was quantified with QTLtools "quan" on the STAR-aligned bam files (see above). Association tests between exon expression and Chr1:93,954,637 were conducted with a linear model in R that considered three PCs, age, and RIN as covariates. Bonferroni correction was applied to determine a significance threshold with 0.05/n, where n is the number of exons tested.

Data availability

DNA and RNA sequencing data of 118 bulls are available in the ENA database at the study accessions PRJEB28191 and PRJEB46995. Gene expression and splicing matrices, a VCF file of genome-wide genotypes used for e/sQTL mapping, a cross-table to link genotype and transcriptome data, as well as summary statistics used for transcriptome-wide association testing have been archived at zenodo (https://doi.org/10.5281/zenodo.8093287).

Author contributions

XMM sampled tissue and established the molQTL cohort, aligned RNA sequencing data, quantified gene expression and splicing variation, developed workflows and applied them to map e/sQTL, contributed to the TWAS, interpreted results, and drafted the manuscript; NKK imputed sequence variant genotypes, established workflows for GWAS, conducted ASE analyses and TWAS, contributed to eQTL analysis, interpreted results, and contributed to the writing of the manuscript; NKK and XMM performed colocalization analyses; MH coordinated the sampling of tissue with the abattoir staff, sampled tissue, and prepared phenotype data; ALV contributed to short read alignment; ASL performed variant discovery and genotyping; QH contributed to GWAS; MB performed the WASP alignment of the RNA-seq data and contributed to discussions about the molQTL mapping workflows; HP conceptualized the study, contributed to the molQTL fine-mapping, interpreted results, and contributed to the writing of the manuscript; all authors read and approved the final version of the manuscript.

Acknowledgements

We appreciate support from the abattoir veterinarians and staff as well as Till Graf, Patrick Fitzi, and Remo Hengartner for assistance with tissue sampling. We thank Dr. Fritz-Schmitz Hsu and Dr. Ulrich Witschi (Swissgenetics) for providing phenotype data. We thank Braunvieh Schweiz for providing genotype data of Swiss BSW bulls. We acknowledge the Arbeitsgemeinschaft Deutsches Braunvieh, Braunvieh Austria, Tierzuchtforschung Grub, the Chair of Animal Breeding of TU München, the Institute of Animal Breeding from Bayerische Landesanstalt für Landwirtschaft and ZuchtData EDV Dienstleistungen GmbH for providing genotype and phenotype data of Austrian and German BSW bulls. We thank the Functional Genomics Center Zurich (Dr. Catharine Aquino) for generating DNA and RNA sequencing data. We thank Jeremie Vandenplas (Wageningen University & Research,

Wageningen, the Netherlands) for providing a modified version of the GCTA tool that allows considering allele dosage data.

Funding

This study was supported by grants from the Swiss National Science Foundation, an ETH Research Grant, Swissgenetics, and the European Union's Horizon 2020 research and innovation programme under Grant Agreement No. 815668 (BovReg). The funding bodies were neither involved in the design of the study and collection, analysis, and interpretation of data nor in writing the manuscript.

References

Aguet, F., Brown, A. A., Castel, S. E., Davis, J. R., He, Y., Jo, B., Mohammadi, P., Park, Y. S., Parsana, P., Segrè, A. V., Strober, B. J., Zappala, Z., Cummings, B. B., Gelfand, E. T., Hadley, K., Huang, K. H., Lek, M., Li, X., Nedzel, J. L., … Zhu, J. (2017). Genetic effects on gene expression across human tissues. *Nature*, *550*(7675), 204–213. https://doi.org/10.1038/nature24277

Barbeira, A. N., Dickinson, S. P., Bonazzola, R., Zheng, J., Wheeler, H. E., Torres, J. M., Torstenson, E. S., Shah, K. P., Garcia, T., Edwards, T. L., Stahl, E. A., Huckins, L. M., Aguet, F., Ardlie, K. G., Cummings, B. B., Gelfand, E. T., Getz, G., Hadley, K., Handsaker, R. E., … Im, H. K. (2018). Exploring the phenotypic consequences of tissue specific gene expression variation inferred from GWAS summary statistics. *Nature Communications*, *9*(1), 1–20. https://doi.org/10.1038/s41467-018-03621-1

Bray, N. L., Pimentel, H., Melsted, P., & Pachter, L. (2016). Near-optimal probabilistic RNA-seq quantification. *Nature Biotechnology*, *34*(5), 525–527. https://doi.org/10.1038/nbt.3519

Browning, B. L., Tian, X., Zhou, Y., & Browning, S. R. (2021). Fast two-stage phasing of large-scale sequence data. *American Journal of Human Genetics*, *108*(10), 1880–1890. https://doi.org/10.1016/j.ajhg.2021.08.005

Butler, M. L., Bormann, J. M., Weaber, R. L., Grieger, D. M., & Rolf, M. M. (2020). Selection for bull fertility: A review. *Translational Animal Science*, *4*(1), 423–441. https://doi.org/10.1093/TAS/TXZ174

Castel, S. E., Mohammadi, P., Chung, W. K., Shen, Y., & Lappalainen, T. (2016). Rare variant phasing and haplotypic expression from RNA sequencing with phASER. *Nature Communications*, *7*. https://doi.org/10.1038/ncomms12817

Chang, C. C., Chow, C. C., Tellier, L. C. A. M., Vattikuti, S., Purcell, S. M., & Lee, J. J. (2015). Second-generation PLINK: Rising to the challenge of larger and richer datasets. *GigaScience*, *4*(1). https://doi.org/10.1186/s13742-015-0047-8

Chen, S., Zhou, Y., Chen, Y., & Gu, J. (2018). Fastp: An ultra-fast all-in-one FASTQ preprocessor. *Bioinformatics*, *34*(17), i884–i890. https://doi.org/10.1093/bioinformatics/bty560

Cotto, K. C., Feng, Y.-Y., Ramu, A., Richters, M., Freshour, S. L., Skidmore, Z. L., Xia, H., McMichael, J. F., Kunisaki, J., Campbell, K. M., Chen, T. H.-P., Rozycki, E. B., Adkins, D., Devarakonda, S., Sankararaman, S., Lin, Y., Chapman, W. C., Maher, C. A., Arora, V., … Griffith, M. (2023). Integrated analysis of genomic and transcriptomic data for the discovery of splice-associated variants in cancer. *Nature Communications*, *14*(1), 1589. https://doi.org/10.1038/s41467-023-37266-6

Dam, A. H. D. M., Koscinski, I., Kremer, J. A. M., Moutou, C., Jaeger, A. S., Oudakker, A. R., Tournaye, H., Charlet, N., Lagier-Tourenne, C., Van Bokhoven, H., & Viville, S. (2007). Homozygous mutation in SPATA16 is associated with male infertility in human globozoospermia. *American Journal of Human Genetics*, *81*(4), 813–820. https://doi.org/10.1086/521314

Delaneau, O., Ongen, H., Brown, A. A., Fort, A., Panousis, N. I., & Dermitzakis, E. T. (2017). A complete tool set for molecular QTL discovery and analysis. *Nature Communications*, *8*. https://doi.org/10.1038/ncomms15452

Dobin, A., Davis, C. A., Schlesinger, F., Drenkow, J., Zaleski, C., Jha, S., Batut, P., Chaisson, M., & Gingeras, T. R. (2013). STAR: Ultrafast universal RNA-seq aligner. *Bioinformatics*, *29*(1), 15–21. https://doi.org/10.1093/bioinformatics/bts635

Druet, T., Fritz, S., Sellem, E., Basso, B., Gérard, O., Salas-Cortes, L., Humblot, P., Druart, X., & Eggen, A. (2009). Estimation of genetic parameters and genome scan for 15 semen characteristics traits of Holstein bulls. *Journal of Animal Breeding and Genetics*, *126*(4), 269–277. https://doi.org/10.1111/j.1439-0388.2008.00788.x

Fujihara, Y., Oji, A., Larasati, T., Kojima-Kita, K., & Ikawa, M. (2017). Human globozoospermia-related gene spata16 is required for sperm formation revealed by CRISPR/Cas9-mediated mouse models. *International Journal of Molecular Sciences*, *18*(10). https://doi.org/10.3390/ijms18102208

Garrido-Martín, D., Borsari, B., Calvo, M., Reverter, F., & Guigó, R. (2021). Identification and analysis of splicing quantitative trait loci across multiple tissues in the human genome. *Nature Communications*, *12*(1). https://doi.org/10.1038/s41467-020-20578-2

Gebreyesus, G., Lund, M. S., Kupisiewicz, K., & Su, G. (2021). Genetic parameters of semen quality traits and genetic correlations with service sire nonreturn rate in Nordic Holstein bulls. *Journal of Dairy Science*, *104*(9), 10010–10019. https://doi.org/10.3168/jds.2021-20403

Giambartolomei, C., Vukcevic, D., Schadt, E. E., Franke, L., Hingorani, A. D., Wallace, C., & Plagnol, V. (2014). Bayesian Test for Colocalisation between Pairs of Genetic Association Studies Using Summary Statistics. *PLoS Genetics*, *10*(5). https://doi.org/10.1371/journal.pgen.1004383

GTEx Consortium. (2020). The GTEx Consortium atlas of genetic regulatory effects across human tissues. *Science*, *369*(6509), 1318–1330. www.gtexportal.org

Guo, J., Nie, X., Giebler, M., Mlcochova, H., Wang, Y., Grow, E. J., Kim, R., Tharmalingam, M., Matilionyte, G., Lindskog, C., Carrell, D. T., Mitchell, R. T., Goriely, A., Hotaling, J. M., & Cairns, B. R. (2020). The Dynamic Transcriptional Cell Atlas of Testis Development during Human Puberty. *Cell Stem Cell*, *26*(2), 262-276.e4. https://doi.org/10.1016/j.stem.2019.12.005

Hiltpold, M., Kadri, N. K., Janett, F., Witschi, U., Schmitz-Hsu, F., & Pausch, H. (2021). Autosomal recessive loci contribute significantly to quantitative variation of male fertility in a dairy cattle population. *BMC Genomics*, *22*(1). https://doi.org/10.1186/s12864-021-07523-3

Hiltpold, M., Niu, G., Kadri, N. K., Crysnanto, D., Fang, Z. H., Spengeler, M., Schmitz-Hsu, F., Fuerst, C., Schwarzenbacher, H., Seefried, F. R., Seehusen, F., Witschi, U., Schnieke, A., Fries, R., Bollwein, H., Flisikowski, K., & Pausch, H. (2020). Activation of cryptic splicing in bovine WDR19 is associated with reduced semen quality and male fertility. *PLoS Genetics*, *16*(5). https://doi.org/10.1371/journal.pgen.1008804

Kaessmann, H. (2010). Origins, evolution, and phenotypic impact of new genes. In *Genome Research* (Vol. 20, Issue 10, pp. 1313–1326). https://doi.org/10.1101/gr.101386.109

Lamas-Toranzo, I., Hamze, J. G., Bianchi, E., Fernández-Fuertes, B., Pérez-Cerezales, S., Laguna-Barraza, R., Fernández-González, R., Lonergan, P., Gutiérrez-Adán, A., Wright, G. J., Jiménez-Movilla, M., & Bermejo-álvarez, P. (2020). TMEM95 is a sperm membrane protein essential for mammalian fertilization. *ELife*, *9*, 1–18. https://doi.org/10.7554/eLife.53913

Leonard, A. S., Crysnanto, D., Mapel, X. M., Bhati, M., & Pausch, H. (2023). Graph construction method impacts variation representation and analyses in a bovine super-pangenome. *Genome Biology*, *24*(1), 124. https://doi.org/10.1186/s13059-023-02969-y

Leonard, A. S., Mapel, X. M., & Pausch, H. (2023). Pangenome genotyped structural variation improves molecular phenotype mapping in cattle. *BioRxiv*. https://doi.org/10.1101/2023.06.21.545879

Li, H. (2013). *Aligning sequence reads, clone sequences and assembly contigs with BWA-MEM*. http://arxiv.org/abs/1303.3997

Li, Y. I., Knowles, D. A., Humphrey, J., Barbeira, A. N., Dickinson, S. P., Im, H. K., & Pritchard, J. K. (2018). Annotation-free quantification of RNA splicing using LeafCutter. *Nature Genetics*, *50*(1), 151–158. https://doi.org/10.1038/s41588-017-0004-9

Li, Y. I., Van De Geijn, B., Raj, A., Knowles, D. A., Petti, A. A., Golan, D., Gilad, Y., & Pritchard, J. K. (2016). RNA splicing is a primary link between genetic variation and disease. *Science*, *352*(6285), 600–604. https://www.science.org

Liao, Y., Smyth, G. K., & Shi, W. (2014). FeatureCounts: An efficient general purpose program for assigning sequence reads to genomic features. *Bioinformatics*, *30*(7), 923–930. https://doi.org/10.1093/bioinformatics/btt656

Liu, S., Gao, Y., Canela-Xandri, O., Wang, S., Yu, Y., Cai, W., Li, B., Xiang, R., Chamberlain, A. J., Pairo-Castineira, E., D'Mellow, K., Rawlik, K., Xia, C., Yao, Y., Navarro, P., Rocha, D., Li, X., Yan, Z., Li,

C., … Fang, L. (2022a). A multi-tissue atlas of regulatory variants in cattle. *Nature Genetics*, *54*(9), 1438–1447. https://doi.org/10.1038/s41588-022-01153-5

Liu, S., Gao, Y., Canela-Xandri, O., Wang, S., Yu, Y., Cai, W., Li, B., Xiang, R., Chamberlain, A. J., Pairo-Castineira, E., D'Mellow, K., Rawlik, K., Xia, C., Yao, Y., Navarro, P., Rocha, D., Li, X., Yan, Z., Li, C., … Fang, L. (2022b). A multi-tissue atlas of regulatory variants in cattle. *Nature Genetics*. https://doi.org/10.1038/s41588-022-01153-5

Liu, S., Ma, X., Wang, Z., Lin, F., Li, M., Li, Y., Yang, L., Rushdi, H. E., Riaz, H., Gao, T., Yang, L., Fu, T., & Deng, T. (2023). MAEL gene contributes to bovine testicular development through the m5C-mediated splicing. *IScience*, *26*(2). https://doi.org/10.1016/j.isci.2023.105941

Love, M. I., Huber, W., & Anders, S. (2014). Moderated estimation of fold change and dispersion for RNA-seq data with DESeq2. *Genome Biology*, *15*(12). https://doi.org/10.1186/s13059-014-0550-8

McLaren, W., Gil, L., Hunt, S. E., Riat, H. S., Ritchie, G. R. S., Thormann, A., Flicek, P., & Cunningham, F. (2016). The Ensembl Variant Effect Predictor. *Genome Biology*, *17*(1). https://doi.org/10.1186/s13059-016-0974-4

Mohammadi, P., Castel, S. E., Brown, A. A., & Lappalainen, T. (2017). Quantifying the regulatory effect size of cis-acting genetic variation using allelic fold change. *Genome Research*, *27*(11), 1872–1884. https://doi.org/10.1101/gr.216747.116

Murat, F., Mbengue, N., Winge, S. B., Trefzer, T., Leushkin, E., Sepp, M., Cardoso-Moreira, M., Schmidt, J., Schneider, C., Mößinger, K., Brüning, T., Lamanna, F., Belles, M. R., Conrad, C., Kondova, I., Bontrop, R., Behr, R., Khaitovich, P., Pääbo, S., … Kaessmann, H. (2023). The molecular evolution of spermatogenesis across mammals. *Nature*, *613*(7943), 308–316. https://doi.org/10.1038/s41586-022-05547-7

Nagai, R., Kinukawa, M., Watanabe, T., Ogino, A., Kurogi, K., Adachi, K., Satoh, M., & Uemoto, Y. (2022). Genome-wide detection of non-additive quantitative trait loci for semen production traits in beef and dairy bulls. *Animal*, *16*(3). https://doi.org/10.1016/j.animal.2022.100472

Oura, S., Koyano, T., Kodera, C., Yuki Horisawa-Takada, Matsuyama, M., Ishiguro, K. I., & Ikawa, M. (2021). KCTD19 and its associated protein ZFP541 are independently essential for meiosis in male mice. *PLoS Genetics*, *17*(5 May). https://doi.org/10.1371/journal.pgen.1009412

Pausch, H., Kölle, S., Wurmser, C., Schwarzenbacher, H., Emmerling, R., Jansen, S., Trottmann, M., Fuerst, C., Götz, K. U., & Fries, R. (2014). A Nonsense Mutation in TMEM95 Encoding a Nondescript Transmembrane Protein Causes Idiopathic Male Subfertility in Cattle. *PLoS Genetics*, *10*(1). https://doi.org/10.1371/journal.pgen.1004044

Pausch H, Mapel XM. Review: Genetic mutations affecting bull fertility. *Animal*, in press

Pirinen, M., Lappalainen, T., Zaitlen, N. A., Dermitzakis, E. T., Donnelly, P., McCarthy, M. I., & Rivas, M. A. (2015). Assessing allele-specific expression across multiple tissues from RNA-seq read data. *Bioinformatics*, *31*(15), 2497–2504. https://doi.org/10.1093/bioinformatics/btv074

Poplin, R., Chang, P. C., Alexander, D., Schwartz, S., Colthurst, T., Ku, A., Newburger, D., Dijamco, J., Nguyen, N., Afshar, P. T., Gross, S. S., Dorfman, L., McLean, C. Y., & Depristo, M. A. (2018). A universal snp and small-indel variant caller using deep neural networks. *Nature Biotechnology*, *36*(10), 983. https://doi.org/10.1038/nbt.4235

Ramsköld, D., Wang, E. T., Burge, C. B., & Sandberg, R. (2009). An abundance of ubiquitously expressed genes revealed by tissue transcriptome sequence data. *PLoS Computational Biology*, *5*(12). https://doi.org/10.1371/journal.pcbi.1000598

Rezende, F. M., Dietsch, G. O., & Peñagaricano, F. (2018). Genetic dissection of bull fertility in US Jersey dairy cattle. *Animal Genetics*, *49*(5), 393–402. https://doi.org/10.1111/age.12710

Rosen, B. D., Bickhart, D. M., Schnabel, R. D., Koren, S., Elsik, C. G., Tseng, E., Rowan, T. N., Low, W. Y., Zimin, A., Couldrey, C., Hall, R., Li, W., Rhie, A., Ghurye, J., McKay, S. D., Thibaud-Nissen, F., Hoffman, J., Murdoch, B. M., Snelling, W. M., … Medrano, J. F. (2020). De novo assembly of the cattle reference genome with single-molecule sequencing. *GigaScience*, *9*(3). https://doi.org/10.1093/gigascience/giaa021

Soumillon, M., Necsulea, A., Weier, M., Brawand, D., Zhang, X., Gu, H., Barthès, P., Kokkinaki, M., Nef, S., Gnirke, A., Dym, M., deMassy, B., Mikkelsen, T. S., & Kaessmann, H. (2013). Cellular Source and Mechanisms of High Transcriptome Complexity in the Mammalian Testis. *Cell Reports*, *3*(6), 2179–2190. https://doi.org/10.1016/j.celrep.2013.05.031

Stegle, O., Parts, L., Piipari, M., Winn, J., & Durbin, R. (2012). Using probabilistic estimation of expression residuals (PEER) to obtain increased power and interpretability of gene expression analyses. *Nature Protocols*, *7*(3), 500–507. https://doi.org/10.1038/nprot.2011.457

Tang, S., Lu, Y., Skinner, W. M., Sanyal, M., Lishko, P. V, Ikawa, M., & Kim, P. S. (2022). *Human sperm TMEM95 binds eggs and facilitates membrane fusion BIOPHYSICS AND COMPUTATIONAL BIOLOGY OPEN ACCESS*. https://doi.org/10.1073/pnas

Tarasov, A., Vilella, A. J., Cuppen, E., Nijman, I. J., & Prins, P. (2015). Sambamba: fast processing of NGS alignment formats. *Bioinformatics*, *31*(12), 2032–2034. https://doi.org/10.5281/zenodo.13200

The FarmGTEx-PigGTEx Consortium, Teng, J., Gao, Y., Yin, H., Bai, Z., Liu, S., Zeng, H., Bai, L., Cai, Z., Zhao, B., Xu, Z., Lin, Q., Pan, Z., Yang, W., Yu, X., Hou, Y., Keel, B. N., Rohrer, G. A., Lindholm-Perry, A. K., … Fang, L. (2022). A compendium of genetic regulatory effects across pig tissues. *BioRxiv*. https://doi.org/10.1101/2022.11.11.516073

Thibier, M., & Wagner, H.-G. (2002). World statistics for artificial insemination in cattle. In Livestock Production Science (Vol. 74). www.elsevier.com/locate/livprodsci

Tüttelmann, F., Ruckert, C., & Röpke, A. (2018). Spermatogenesestörungen: Perspektiven für erweiterte genetische Diagnostik nach 20 Jahren unveränderter Routine. Medizinische Genetik, 30(1), 12–20. https://doi.org/10.1007/s11825-018-0181-7

Urbut, S. M., Wang, G., Carbonetto, P., & Stephens, M. (2019). Flexible statistical methods for estimating and testing effects in genomic studies with multiple conditions. *Nature Genetics*, *51*(1), 187–195. https://doi.org/10.1038/s41588-018-0268-8

Van De Geijn, B., Mcvicker, G., Gilad, Y., & Pritchard, J. K. (2015). WASP: Allele-specific software for robust molecular quantitative trait locus discovery. In *Nature Methods* (Vol. 12, Issue 11, pp. 1061–1063). Nature Publishing Group. https://doi.org/10.1038/nmeth.3582

Wainberg, M., Sinnott-Armstrong, N., Mancuso, N., Barbeira, A. N., Knowles, D. A., Golan, D., Ermel, R., Ruusalepp, A., Quertermous, T., Hao, K., Björkegren, J. L. M., Im, H. K., Pasaniuc, B., Rivas, M. A., & Kundaje, A. (2019). Opportunities and challenges for transcriptome-wide association studies. *Nature Genetics*, *51*(4), 592–599. https://doi.org/10.1038/s41588-019-0385-z

Walker, R. L., Ramaswami, G., Hartl, C., Mancuso, N., Gandal, M. J., de la Torre-Ubieta, L., Pasaniuc, B., Stein, J. L., & Geschwind, D. H. (2019). Genetic Control of Expression and Splicing in Developing Human Brain Informs Disease Mechanisms. *Cell*, *179*(3), 750-771.e22. https://doi.org/10.1016/j.cell.2019.09.021

Wang, S., Qiao, H., Wang, P., Wang, Y., & Qin, D. (2021). ZDHHC19 is dispensable for spermatogenesis, but is essential for sperm functions in mice. *International Journal of Molecular Sciences*, *22*(16). https://doi.org/10.3390/ijms22168894

Wang, W., Su, L., Meng, L., He, J., Tan, C., Yi, D., Cheng, D., Zhang, H., Lu, G., Du, J., Lin, G., Zhang, Q., Tu, C., & Tan, Y.-Q. (2023). Biallelic variants in KCTD19 associated with male factor infertility and oligoasthenoteratozoospermia. *Human Reproduction*. https://doi.org/10.1093/humrep/dead095

Wu, Y., Broadaway, K. A., Raulerson, C. K., Scott, L. J., Pan, C., Ko, A., He, A., Tilford, C., Fuchsberger, C., Locke, A. E., Stringham, H. M., Jackson, A. U., Narisu, N., Kuusisto, J., Pajukanta, P., Collins, F. S., Boehnke, M., Laakso, M., Lusis, A. J., … Mohlke, K. L. (2019). Colocalization of GWAS and eQTL signals at loci with multiple signals identifies additional candidate genes for body fat distribution. *Human Molecular Genetics*, *28*(24), 4161–4172. https://doi.org/10.1093/hmg/ddz263

Xavier, M. J., Salas-Huetos, A., Oud, M. S., Aston, K. I., & Veltman, J. A. (2021). Disease gene discovery in male infertility: past, present and future. In Human Genetics (Vol. 140, Issue 1, pp.

7–19). Springer Science and Business Media Deutschland GmbH. https://doi.org/10.1007/s00439-020-02202-x

Xiang, R., Fang, L., Liu, S., Macleod, I. M., Liu, Z., Breen, E. J., Gao, Y., Liu, G. E., Tenesa, A., Consortium, C., Mason, B. A., Chamberlain, A. J., Wray, N. R., & Goddard, M. E. (2022). Gene expression and RNA splicing explain large proportions of the heritability for complex traits in cattle. *BioRxiv*. https://doi.org/10.1101/2022.05.30.494093

Yamaguchi, K., Ishigaki, K., Suzuki, A., Tsuchida, Y., Tsuchiya, H., Sumitomo, S., Nagafuchi, Y., Miya, F., Tsunoda, T., Shoda, H., Fujio, K., Yamamoto, K., & Kochi, Y. (2022). Splicing QTL analysis focusing on coding sequences reveals mechanisms for disease susceptibility loci. *Nature Communications*, *13*(1). https://doi.org/10.1038/s41467-022-32358-1

Yang, J., Lee, S. H., Goddard, M. E., & Visscher, P. M. (2011). GCTA: A tool for genome-wide complex trait analysis. *American Journal of Human Genetics*, *88*(1), 76–82. https://doi.org/10.1016/j.ajhg.2010.11.011

Yun, T., Li, H., Chang, P. C., Lin, M. F., Carroll, A., & McLean, C. Y. (2020). Accurate, scalable cohort variant calls using DeepVariant and GLnexus. *Bioinformatics*, *36*(24), 5582–5589. https://doi.org/10.1093/bioinformatics/btaa1081